Aspects of phonon spectra for classical Gaussian core models

Frank H. Stillinger

Department of Chemistry, Princeton University, Princeton, New Jersey 08544, USA

Calculations have focused on several key aspects of phonon spectra for the stable lattice structures of the Gaussian core model. These structures include the linear array ($D=1$), the close-packed triangular lattice ($D=2$), and the low-density face-centered and high-density body-centered-cubic lattices ($D=3$). In each dimension, compressing the system isotropically eventually causes strong depression of phonon frequencies for wave vectors approaching the Brillouin zone boundary, and this depression moves inward toward the **k**-space origin with increasing compression. Phonon spectra for uniformly shear-strained triangular lattices illustrate the development of mechanical instability for those systems, also with increasing compression. For $D=3$, the unstrained face-centered-cubic lattice exhibits an upper density limit of mechanical stability owing to development of a "soft" long-wavelength transverse mode and the unstrained body-centered-cubic lattice displays an analogous lower density limit due to a corresponding "soft" long-wavelength transverse mode; furthermore, those upper and lower limiting densities satisfy the basic Gaussian core model duality relation. Finally, these various phonon characteristics are tied to the negative thermal expansions possessed by the model and to the density-dependent potential energy landscape as it relates to the melting transition.

PACS number(s): 63.20.Dj, 65.40.De, 05.20.−y

I. INTRODUCTION

When it is expressed in natural energy and length units, the N-particle interaction function that defines a Gaussian core model (GCM) in space dimension D has the followng pairwise additive form:

$$\Phi(\mathbf{r}_1 \cdots \mathbf{r}_N) = \sum_{i<j} \exp(- r_{ij}{}^2). \qquad (1.1)$$

Formally, this describes a set of structureless, spherically symmetrical particles. However, one of the motivating reasons for examining a GCM is that it represents an idealized version of interacting linear polymer molecules in a suitable solvent medium, a fact first evident in the work of Flory and Krigbaum[1] and supported more recently by both analytical studies[2,3] and computer simulation.[3] Furthermore, Gaussian pair interactions also appear to be an appropriate description for the family of flexible dendrimers (recursively branched polymers).[2] In these interpretations, each $\mathbf{r}_i$ in Eq. (1.1) above is the position of a molecular "center." Although these polymer connections nominally identify the continuous GCM as belonging in $D=3$ dimensions, it has nevertheless been useful from the analytical viewpoint to study this model for other values of D.[4–8]

Prior studies of the GCM, including both analytical and simulational approaches, have established several remarkable properties. These include (a) a reduction to the hard sphere (or disk or rod) system in the low-density, low-temperature limit;[9] (b) the existence of an exact duality relation that connects $T=0$ lattice energies at conjugate low and high densities;[8] (c) the equivalence of any density increase to a convolution smoothing operation applied to the multidimensional "rugged landscape" for potential energy Φ, thereby reducing its collection of inherent structures (local Φ minima) (Ref. 10); (d) the presence of a single melting temperature maximum versus density or pressure,[3,9] as well as

crystal and fluid phase regions of negative thermal expansion (for $D=2,3$) (Refs. 6 and 10); (e) the decline of the melting temperature to zero (for $D=2$ and 3) as density increases;[3,9] and (f) an asymptotic reduction of properties of the high-density fluid phase to those predicted by the hypernetted chain[3] (HNC) and mean-field[11] (MF) approximations.

The present paper is devoted to an examination of selected aspects of the GCM phonon spectra. Of course these phonons cannot literally represent the dynamics for a collection of polymers suspended in a viscous solvent. However, they do determine the absolute entropy and free energy of the ordered states of the idealized GCM in every dimension and thus are basic for locating phase transitions in connection with high-temperature expansions.[5] As we shall see below, the phonon spectra for GCM's have some unusual features that are logically connected to points (b), (c), and (e) above.

Section II initiates the present study by calculating the frequencies of harmonic normal modes (phonons) for the regular linear array ($D=1$). The conventional dispersion relation for $\omega(k)$ is numerically easy to evaluate at low density, but becomes increasingly cumbersome to use as the density increases. Fortunately, the theory of Jacobi θ functions (details in the Appendix) offers a transformation that is roughly analogous to the duality relation mentioned in point (b) above and which greatly facilitates extraction of the high-density $\omega(k)$. The results exhibit a peculiar phenomenon; specifically, the phonon frequencies at and near the Brillouin zone boundary drop precipitously toward zero with increasing density. This has the effect of producing a k-space interval over which phase and group velocities have opposite directions.

Section III presents results for the $D=2$ GCM, for which the regular triangular lattice is the most stable configuration at all densities. In a manner analogous to that observed for $D=1$, one of the phonon branches (longitudinal) displays a precipitous frequency decline at and near the Brillouin zone

boundary as the density increases. The other (transverse) branch in fact is strongly depressed at all wave vectors by the density increase. These phenomena are connected with the potential landscape self-smoothing characteristic mentioned in point (c) above.

Section IV contains a variant of the $D=2$ analysis, involving the effect of uniform anisotropic strains on the triangular lattice. Producing these strains costs energy, of course, and moves the system out of its global potential minimum into a higher-lying relative minimum. Diagonalization of the secular equation reveals the appearance of imaginary frequencies when the magnitude of the strain exceeds a density-dependent magnitude. Such imaginary frequencies indicate instability of the strained-lattice inherent structures in favor of less strained versions, just as point (c) above demands. In terms of the multidimensional potential energy "landscape," the appearance of imaginary frequencies signals the conversion of inherent structures to saddle points, as they are absorbed into neighboring inherent-structure basins.

Section V considers $D=3$, for which the stable crystal form is face-centered cubic at low density and body-centered cubic at high density.[3,9] The latter once again exhibits a dramatic compression-induced frequency drop within the phonon dispersion relation. This feature constitutes a substantial breakdown of the Debye approximation for the vibrational spectrum,[12] a comment also applicable to the $D=1$ and $D=2$ cases. Even without the influence of uniform anisotropic strain, the face-centered-cubic crystal develops imaginary-frequency instability as the density rises into the metastable density regime for that structure. Inversely, the body-centered-cubic crystal becomes unstable as it is expanded below its lowest density of stability. The respective densities of first-encountered instability satisfy the aforementioned duality, point (b) above, owing to a connection to elastic constants for the two cubic structures.

The closing section VI summarizes results, discusses a few implications and related issues, and suggests some topics for future research.

II. LINEAR CHAIN ($D=1$)

In each of the phonon spectrum calculations to be presented in this and the following sections, periodic boundary conditions will apply. The ground-state array for N particles along a line interval of length L thus will be free to translate. Prior to imposition of a phonon disturbance, the N particles are arranged in numerical sequence at the time-independent positions

$$x_j^{(0)} = jL/N \quad (1 \leq j \leq N). \tag{2.1}$$

Because the primary interest lies in the large-system limit, it may be supposed that L far exceeds the range of the Gaussian pair potential, even at high number density $\rho = N/L$. A phonon of wave vector k involves perturbing the positions (2.1) to the time-dependent locations

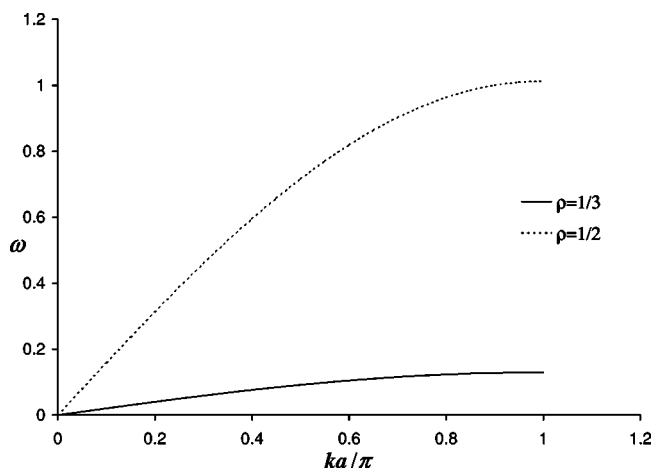$$x_j(t) = x_j^{(0)} + A(k)\exp[ikx_j^{(0)} - i\omega(k)t],$$

FIG. 1. Phonon frequencies for the linear ($D=1$) GCM, at the two relatively low number densities $1/3$ and $1/2$.

$$k = 2\pi n/L \quad (0 \leq n \leq N-1). \tag{2.2}$$

Here $\omega(k)$ is the angular frequency and the phonon amplitude $A(k)$ must be small to remain in the regime of harmonic motions (independent phonons).

The force experienced by each particle j follows from the corresponding gradient of potential energy Φ, Eq. (1.1), evaluated at the displaced positions, Eq. (2.2). Using these forces in the Newtonian equations of motion and after linearizing with respect to amplitude $A(k)$, one finally obtains an equation for determining the $\omega(k)$ dispersion relation. Assuming for this and all subsequent calculations that all particles have unit mass, the determining equation has the following form:

$$\omega^2(k) = 4\sum_{l=1}^{\infty} [2(l/\rho)^2 - 1][1 - \cos(kl/\rho)]\exp(-l^2/\rho^2). \tag{2.3}$$

Figure 1 presents $\omega(k)$ plots computed from this equation for two relatively low densities, $\rho=1/3$ and $1/2$, showing for each a simple monotonic rise as k increases from 0 to the Brillouin zone boundary[13] at $k/\rho = \pi$, as well as a strong positive density dependence at fixed k.

As the particle density ρ increases, the number of terms on the right-hand side of Eq. (2.3) required to attain a given numerical precision also increases. Furthermore, a qualitative change in the form of $\omega(k)$ appears when ρ exceeds approximately unity. Specifically, $\omega(k)$ develops a maximum within the Brillouin zone, and declines in value as k approaches the zone boundary. Figure 2 illustrates this phenomenon for $\rho=2$ and 5. While the initial slope of $\omega(k)$ at the origin continues to increase with density, the maximum moves inward toward the origin, and frequencies beyond the maximum plunge strongly toward zero. It may be worth reminding the reader that the group velocity of a wave packet of phonons is determined by $\partial\omega/\partial k$,[13] and because this shows a sign reversal, phonon phase velocities and group velocities for k's beyond the maximum travel in opposite directions.
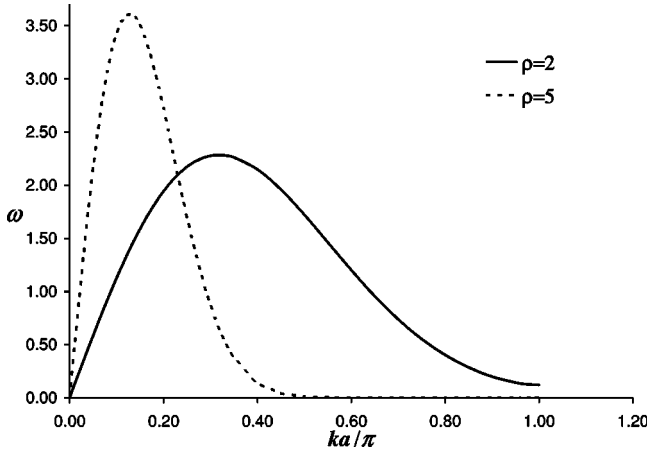
FIG. 2. Phonon frequencies for the linear ($D=1$) GCM at number densities 2 and 5. These cases illustrate the development of a frequency maximum within the Brillouin zone in the high-density regime.

The determining equation (2.3) can be transformed into an alternative form, using results from the theory of Jacobi θ functions,[14] so that it is better adapted to describe the high-density limit of the one-dimensional GCM. Details appear in the Appendix. That alternative form is the following:

$$\omega^2(k) = \pi^{1/2}\rho k^2 \exp(-k^2/4) - 4\pi^{1/2}\rho \sum_{l=1}^{\infty} \exp(-\pi^2\rho^2 l^2)$$
$$\times \{2\pi^2\rho^2 l^2 + \exp(-k^2/4)[2\pi\rho k l \sinh(\pi\rho k l)$$
$$- (k^2/2 + 2\pi^2\rho^2 l^2)\cosh(\pi\rho k l)]\}. \quad (2.4)$$

Whereas more and more terms were necessary to evaluate the right-hand side of Eq. (2.3) to given precision for nonzero k as density increased, the reverse is true for the transformed version (2.4). In fact, for fixed $k>0$, the asymptotic behavior in the high-density limit emerges from the leading term in Eq. (2.4) alone:

$$\omega(k) \sim \pi^{1/4}\rho^{1/2}|k|\exp(-k^2/8) \quad (\rho \to \infty) \quad (2.5)$$

At the zone boundary,

$$\omega(k = \pi\rho) \sim \pi^{5/4}\rho^{3/2} \exp(-\pi^2\rho^2/8). \quad (2.6)$$

III. REGULAR TRIANGULAR LATTICE ($D=2$)

The position vectors of all N particles in the undisturbed triangular lattice are generated as integer multiples of basis vectors $\mathbf{b}_1$ and $\mathbf{b}_2$:

$$\mathbf{r}_j^{(0)} = n_1(j)\mathbf{b}_1 + n_2(j)\mathbf{b}_2, \quad (3.1)$$

where

$$\mathbf{b}_1 = a\mathbf{u}_x,$$

$$\mathbf{b}_2 = a[(1/2)\mathbf{u}_x + (3^{1/2}/2)\mathbf{u}_y]. \quad (3.2)$$

Here $\mathbf{u}_x$ and $\mathbf{u}_y$ are unit vectors for the x, y Cartesian coordinate system aligned with the principal directions of the lat-

tice and a is the nearest-neighbor separation at number density ρ:

$$a(\rho) = [2/(3^{1/2}\rho)]^{1/2}. \quad (3.3)$$

As stated earlier, periodic boundary conditions apply to this two-dimensional system of N particles.

Phonons with wave vector $\mathbf{k}$ and angular frequency $\omega(\mathbf{k})$ will be described by the following generic set of displaced positions:

$$\mathbf{r}_j(t) = \mathbf{r}_j^{(0)} + \mathbf{A}(\mathbf{k})\exp[i\mathbf{k}\cdot\mathbf{r}_j^{(0)} - i\omega(\mathbf{k})t]. \quad (3.4)$$

Upon inserting this form into the coupled Newton equations of motion for the N particles of the lattice, there emerges a pair of homogeneous equations that must be satisfied by the components $A_x(\mathbf{k})$ and $A_y(\mathbf{k})$ of the amplitude vector $\mathbf{A}(\mathbf{k})$:

$$0 = [(1/2)\omega^2 + \sigma_1 - 2\sigma_{xx}]A_x - 2\sigma_{xy}A_y,$$

$$0 = -2\sigma_{xy}A_x + [(1/2)\omega^2 + \sigma_1 - 2\sigma_{yy}]A_y, \quad (3.5)$$

where

$$\sigma_1(\mathbf{k}) = \sum_j [1 - \cos(\mathbf{k}\cdot\mathbf{r}_j)]\exp(-r_j^2),$$

$$\sigma_{xx}(\mathbf{k}) = \sum_j x_j^2[1 - \cos(\mathbf{k}\cdot\mathbf{r}_j)]\exp(-r_j^2),$$

$$\sigma_{xy}(\mathbf{k}) = \sigma_{yx}(\mathbf{k}) = \sum_j x_j y_j[1 - \cos(\mathbf{k}\cdot\mathbf{r}_j)]\exp(-r_j^2),$$

$$\sigma_{yy}(\mathbf{k}) = \sum_j y_j^2[1 - \cos(\mathbf{k}\cdot\mathbf{r}_j)]\exp(-r_j^2). \quad (3.6)$$

In each of these four sums, j indexes all undisplaced lattice positions relative to a fixed lattice site.

The pair of equations (3.5) is compatible only if the determinant of coefficients vanishes, which leads to the following expression for the two phonon branches at each wave vector $\mathbf{k}$:

$$\omega^2(\mathbf{k})/2 = \sigma_{xx}(\mathbf{k}) + \sigma_{yy}(\mathbf{k}) - \sigma_1(\mathbf{k})$$
$$\pm \{[\sigma_{xx}(\mathbf{k}) - \sigma_{yy}(\mathbf{k})]^2 + 4\sigma_{xy}^2(\mathbf{k})\}^{1/2}. \quad (3.7)$$

The angular frequency function $\omega(\mathbf{k})$ for this two-dimensional example is doubly periodic. Its Brillouin zone (fundamental period) is a regular hexagon in $\mathbf{k}$ space, surrounding the origin, with side length equal to[13]

$$4\pi/3a = 2^{3/2}\rho^{1/2}/3^{3/4}. \quad (3.8)$$

Figure 3 shows the first Brillouin zone for the given choice of lattice orientation, Eqs. (3.1) and (3.2). This zone and its periodic images are the Voronoi (nearest-neighbor) polygons for the reciprocal lattice in $\mathbf{k}$ space, which is also triangular.[13]

Numerical solutions to the determining Eq. (3.7) have been exhaustively studied throughout the Brillouin zone for densities in the range $0 < \rho \le 5$. The upper and lower signs in Eq. (3.7) correspond to phonons that at small $\mathbf{k}$ exhibit longitudinal and transverse polarizations, respectively. Conse-
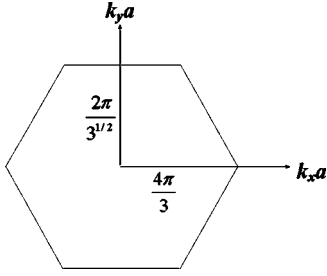
FIG. 3. First Brillouin zone for the triangular-lattice ground state of the two-dimensional GCM. The nearest-neighbor spacing has been denoted by a, Eq. (3.8).

quently we shall label the frequencies of these branches by the symbols $\omega_l(\mathbf{k})$ and $\omega_t(\mathbf{k})$. In addition to the trivial case of degeneracy at the origin, these two phonon branches become degenerate for all densities at the vertices of the hexagonal Brillouin zone (e.g., $k_x a = 4\pi/3$, $k_y a = 0$).

The transverse phonon branch $\omega_t(\mathbf{k})$ is found to be monotonically increasing, at every density, along any ray that extends from the origin to the zone boundary. However, the same is not the case for the longitudinal branch $\omega_l(\mathbf{k})$, which at least in some ray directions at all densities passes through a maximum before reaching the zone boundary. In fact, this behavior appears along every ray at sufficiently high density, with strong depressions in frequencies at the boundary. These depressions increase in severity with increasing density, although all $\mathbf{k} > 0$ frequencies remain positive. In this respect the longitudinal modes are analogous to the $D=1$ phonon branch discussed in the preceding section II. Figure 4 offers an illustrative example, where both branches are plotted along the ray $k_x \geq 0, k_y = 0$, for the relatively high density $\rho = 2$.

Evidently these phenomena stem from the convolution smoothing property, point (c) in the Introduction, that links density increase to a reduction in barriers between neighboring potential energy basins in the multidimensional configuration space for the system and, by implication, to a reduction in at least some harmonic force constants at the surviving basin minima.
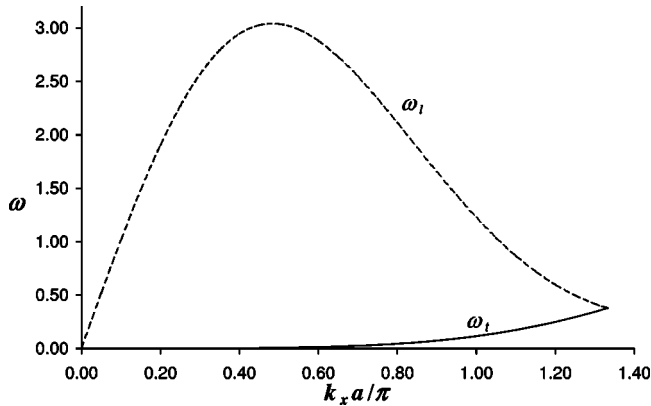

FIG. 4. Plots of frequencies of the two phonon branches for the planar GCM at number density 2, along the ray $k_x \geq 0, k_y = 0$. The ratio of slopes (group velocities) near the origin in this case is approximately 3000.

IV. STRAINED TRIANGULAR LATTICE ($D=2$)

The next objective is to determine how the phonon spectra of the two-dimensional GCM respond to a uniform strain that does not change the number density. In particular, the case to be considered amounts to the following change in basis vectors from the previous forms Eqs. (3.2) for the unstrained lattice:

$$\mathbf{b}_1(\varepsilon) = a(1 + \varepsilon)\mathbf{u}_x,$$

$$\mathbf{b}_2(\varepsilon) = a\left[\left(\frac{1+\varepsilon}{2}\right)\mathbf{u}_x + \left(\frac{3^{1/2}}{2(1+\varepsilon)}\right)\mathbf{u}_y\right]. \quad (4.1)$$

The parameter ε controls a stretch (or compression) along the x direction and, simultaneously, a compression (or stretch) along the y direction. The interest here involves finite, not infinitesimal, strains. Note that ε and $-\varepsilon$ produce inequivalent states. The basis vectors $\mathbf{K}_1$ and $\mathbf{K}_2$ for the reciprocal (Bragg) lattice are determined by $\mathbf{b}_1$ and $\mathbf{b}_2$ as follows:[15]

$$\mathbf{K}_i \cdot \mathbf{b}_j = 2\pi\delta_{ij}. \quad (4.2)$$

As a result, one has

$$\mathbf{K}_1(\varepsilon) = \left(\frac{4\pi}{3^{1/2}a}\right)\left[\left(\frac{3^{1/2}}{2(1+\varepsilon)}\right)\mathbf{u}_x - \left(\frac{1+\varepsilon}{2}\right)\mathbf{u}_y\right],$$

$$\mathbf{K}_2(\varepsilon) = \left(\frac{4\pi}{3^{1/2}a}\right)(1+\varepsilon)\mathbf{u}_y. \quad (4.3)$$

Consequently, the direction of distortion is rotated by $\pm\pi/2$. Just as the number density ρ of lattice points in $\mathbf{r}$ space remains independent of ε, so too does the density ρ_{rec} of reciprocal lattice points in $\mathbf{k}$ space. The product of direct-lattice and reciprocal-lattice densities for any dimension D has the value

$$\rho\rho_{rec} = (2\pi)^{-D}. \quad (4.4)$$

The first Brillouin zone, illustrated in Fig. 3 as a regular hexagon, experiences distortion for $\varepsilon \neq 0$. Consequently, the vertical distance along the $k_y a$ axis from the origin to the midpoint of the upper edge has become

$$2\pi(1+\varepsilon)/3^{1/2}, \quad (4.5)$$

while the horizontal distance from the origin to the vertex on the positive $k_x a$ axis is now

$$\pi\left[\frac{(1+\varepsilon)^3}{3} + \frac{1}{1+\varepsilon}\right]. \quad (4.6)$$

The prior equation (3.7) for the determination of angular frequencies in the undistorted triangular lattice still remains valid for determination of the $\omega(\mathbf{k}, \varepsilon)$ in the presence of distortion, provided that each of the four σ's that it contains be appropriately generalized. These generalizations simply require that each of the four definitions (3.6) now must incorporate sums over relative particle positions in the strained lattice of interest. As a result of the lattice deformation, the degeneracy of transverse and longitudinal frequencies at the
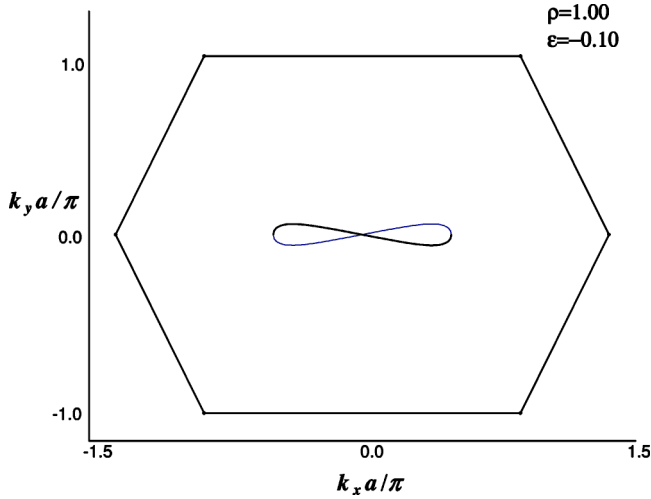
FIG. 5. Two-lobed region for $\rho=1, \varepsilon=-0.1$ within which transverse mode frequencies $\omega_t(\mathbf{k})$ are all imaginary. The longitudinal branch frequencies $\omega_l(\mathbf{k})$ remain real over the entire hexagonal Brillouin zone.

vertices of the Brillouin zone is now removed.

The main objective in this section IV is identification of phonon modes with frequencies forced to become imaginary as a result of lattice distortion. The presence of such imaginary frequencies is equivalent to the existence of instability modes for the periodic lattice structure—i.e., to a loss of status as a mechanically stable inherent structure for the many-particle system. But because every particle in the uniformly strained lattice is a center of symmetry, no particle experiences a net force. Thus $\boldsymbol{\nabla}\boldsymbol{\Phi}=0$ in the $2N$-dimensional configuration space, as was the case before application of the uniform strain. The appearance of imaginary frequencies simply indicates conversion of local $\boldsymbol{\Phi}$ minima (inherent structures) to horizontal saddle points. The number of imaginary frequencies (i.e., the number of directions of negative curvature in the configuration space) determines the order of the saddle point.

Figure 5 provides an illustration. It shows the distorted-hexagon first Brillouin zone for the case $\rho=1$, $\varepsilon=-0.1$. The interior of a small two-lobed region, centered at the origin and shaped roughly like an elongated version of the symbol "∞," contains transverse-mode frequencies $\omega_t(\mathbf{k})$ that are all imaginary. On its boundary these frequencies vanish. Outside of this region the $\omega_t(\mathbf{k})$ are real. By contrast, the longitudinal-branch frequencies $\omega_l(\mathbf{k})$ remain real over the entire Brillouin zone. This example in Fig. 5 amounts to a very high-order saddle if the system is large, because an $O(1)$ fraction of the first Brillouin zone lies within the imaginary-frequency region.

The occurrence of imaginary frequencies for any $0 < \rho < \infty$ requires that the strain magnitude $|\varepsilon|$, both for negative and for positive strains, exceed a density-dependent threshold. For $\rho=1$ and $\varepsilon<0$, detailed calculations reveal that this threshold occurs at approximately $\varepsilon=-0.063$. In contrast, for $\rho=1$ and $\varepsilon>0$, the corresponding threshold occurs at approximately $\varepsilon=0.134$, and when ε exceeds this value, the region containing imaginary $\omega_t(\mathbf{k})$ is centered at the origin,

TABLE I. Strain threshold values at which the $D=2$ triangular lattice becomes unstable.

ρ	ε_-	ε_+
0.10	−0.062	0.100
0.15	−0.076	0.112
0.20	−0.085	0.121
0.25	−0.090	0.127
π^{-1}	−0.092	0.131
0.50	−0.085	0.129
0.75	−0.073	0.128
1.00	−0.063	0.134
1.25	−0.056	0.145
1.50	−0.050	0.158
1.75	−0.046	0.170
2.00	−0.042	0.180

with four lobes that have diagonal orientations. This difference in thresholds and region shapes arises from the fundamental nonequivalence of negative and positive strains as applied to the triangular lattice.

Table I presents a collection of numerically estimated instability thresholds, denoted, respectively, by $\varepsilon_-(\rho)$ and $\varepsilon_+(\rho)$ for negative and positive strains. These results span a factor of 20 in density. A smooth extrapolation suggests that both of these quantities approach zero as the density approaches zero. But in the high-density regime they evidently exhibit diverging behaviors, with $\varepsilon_-(\rho)$ converging to zero, while $\varepsilon_+(\rho)$ appears to increase without limit. It may be significant that both of these threshold functions have extrema at or near the self-dual density $\rho=\pi^{-1}$, an absolute minimum for $\varepsilon_-(\rho)$, and a relative maximum for $\varepsilon_+(\rho)$.

V. THREE-DIMENSIONAL LATTICES

Figures 6(a) and 6(b) illustrate local structures, basis vectors, and coordinate systems that have been used to calculate phonon frequencies for the undistorted low-density face-centered-cubic and high-density body-centered-cubic Bravais lattices. The associated first Brillouin zones are a convex tetradecahedron and dodecahedron, respectively.[13,16] Phonon frequencies for these three-dimensional structures require solving the following triplet of linear homogeneous equations for the components of the polarization vector $\mathbf{A}(\mathbf{k})$:

$$0 = [(1/2)\omega^2 + \sigma_1 - 2\sigma_{xx}]A_x - 2\sigma_{xy}A_y - 2\sigma_{xz}A_z,$$

$$0 = -2\sigma_{xy}A_x + [(1/2)\omega^2 + \sigma_1 - 2\sigma_{yy}]A_y - 2\sigma_{yz}A_z,$$

$$0 = -2\sigma_{xz}A_x - 2\sigma_{yz}A_y + [(1/2)\omega^2 + \sigma_1 - 2\sigma_{zz}]A_z, \quad (5.1)$$

where the various σ's are straightforward extensions of the quantities defined in Eqs. (3.6) above for the two-dimensional lattice. By setting the 3×3 determinant of coefficients in Eqs. (5.1) equal to zero, a cubic equation emerges whose roots are the values of $\omega^2(\mathbf{k})$ for the three
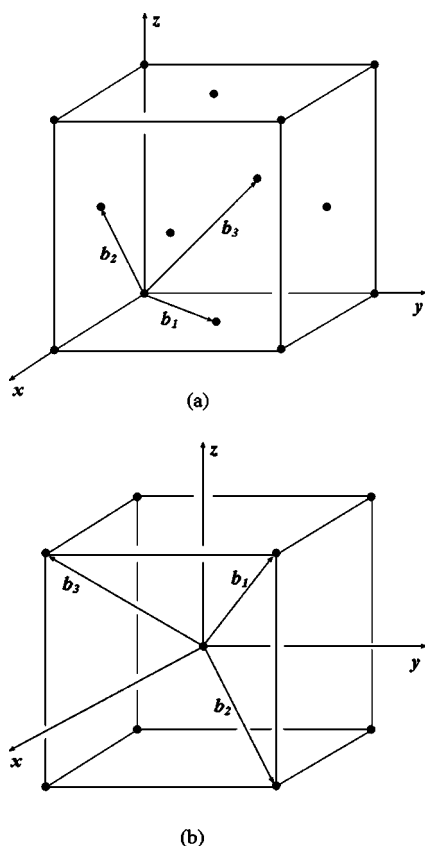
(a)

(b)

FIG. 6. Lattice structures, basis vectors, and coordinate systems used to calculate phonon frequencies for (a) the face-centered-cubic lattice and (b) the body-centered-cubic lattice.

phonon branches. Extensive calculations have been carried out numerically for both the face-centered-cubic and body-centered-cubic lattices, over a wide range of number densities ρ, and throughout the first Brillouin zone. Only a small portion of those results will be reported here.

Along the **k**-space direction $k_x = k_y$, $k_z = 0$, the Brillouin zone boundary for the body-centered-cubic case is encountered at

$$k_x a = k_y a = 3^{1/2}\pi/2, \qquad (5.2)$$

where a denotes the nearest-neighbor distance:

$$a(\rho) = 3^{1/2}/(4\rho)^{1/3}. \qquad (5.3)$$

Along this (110) direction, symmetry dictates that one of the phonon branches retain pure longitudinal character from the origin **k**=0 all the way to the zone boundary, while the other two (nondegenerate) modes retain pure transverse character along the same path. In a manner similar to that observed above in Secs. II and III for the linear array and the undistorted triangular lattice, the longitudinal mode along this ray develops a maximum interior to the Brillouin zone if ρ is sufficiently large. As an example, when $\rho=1.60$ this maximum occurs close to halfway to the zone boundary, with a frequency that is about 1.75 times that at the boundary. Increasing ρ has the effect of moving the position of this longitudinal mode frequency in toward the origin, while increas-

ing its ratio to that at the boundary. Furthermore, the frequencies of all three modes at the boundary decrease with increasing ρ (albeit with distinct rates of decline) provided that $\rho > 0.75$. Because the density range of stability for the face-centered-cubic lattice is much lower, no analogous results exist for that structure.

The same (110) **k**-space direction ($k_x = k_y, k_z = 0$) possesses another important distinction. It is along such a ray, particularly in the $|\mathbf{k}| \to 0$ limit, that the face-centered-cubic particle array loses its mechanical stability as ρ increases. Numerical analysis reveals this instability point to be

$$\rho * (\text{fcc}) \cong 0.3297. \qquad (5.4)$$

This locates the point at which the transverse mode with polarization vector in the x, y plane has its frequency decline to zero. Equivalently, the lattice loses its shear restoring force at this compression. Notice that this instability density considerably exceeds the value $\pi^{-3/2} \cong 0.1796$ at which the face-centered and body-centered structures have equal energies,[8] so metastability precedes instability.

The body-centered-cubic lattice also suffers an analogous mechanical instability, but as a result of decompression. The lower-density limit of mechanical stability has been computationally estimated to be

$$\rho ** (\text{bcc}) \cong 0.09782, \qquad (5.5)$$

which is well below the equal-energy density $\pi^{-3/2}$. Once again this is associated with vanishing of the frequency of a transverse mode with polarization vector in the x, y plane and therefore corresponds to vanishing of shear restoring force. At each of the instability densities ρ^* and ρ^{**}, the numerical analysis reveals that all phonon frequencies $\omega_\alpha(\mathbf{k})$ ($\alpha = 1, 2, 3$) for $\mathbf{k} \neq 0$ remain positive throughout the Brillouin zone.

The shear instabilities of both lattices are associated with a combination of two of the three elastic constants for cubic systems,[17] specifically $\lambda_{xxxx} - \lambda_{xxyy}$. A special feature of the Gaussian core model is that it displays identities that link corresponding properties of the face-centered- and body-centered-cubic structures evaluated at a conjugate pair of dual densities.[8] In particular the above combination of elastic constants satisfies the following identity:[18]

$$\rho^{-3/2}[\lambda_{xxxx}(\rho) - \lambda_{xxyy}(\rho)]_{\text{fcc}} = (\rho')^{-3/2}[\lambda_{xxxx}(\rho') - \lambda_{xxyy}(\rho')]_{\text{bcc}}, \qquad (5.6)$$

where the dual densities are related by

$$\rho\rho' = \pi^{-3}. \qquad (5.7)$$

If the left member of identity (5.6) is evaluated at the face-centered-cubic instability density ρ^*, the square-bracketed factor vanishes by definition. Consequently the corresponding square-bracketed term in the right member must also vanish, with its elastic constants evaluated at the dual density. This implies that

$$\rho * (\text{fcc})\rho ** (\text{bcc}) = \pi^{-3}. \qquad (5.8)$$

Indeed, the numerical estimates (5.4) and (5.5) satisfy this relation, within the four-significant-figure accuracy of those estimates.

VI. CONCLUSIONS AND DISCUSSION

The Gaussian core model presents a specific example of interacting "soft" matter, with constituent particles that are capable of overlap and full interpenetration. This contrasts with more familiar cases, such as the Lennard-Jones model, which exhibit strong and diverging pair repulsion at small separation. It should not be surprising, then, that the Gaussian core model displays unusual collective behavior, specifically as revealed by phonon calculations for its crystal phases. Notable results uncovered during this study include (1) the decline of phonon frequencies as the wave vector **k** increases toward the Brillouin zone boundary, when the model is compressed in one, two, or three dimensions; (2) compression-induced mechanical instabilities of uniformly shear-strained crystal structures in two and three dimensions; and (3) stability upper (fcc) and lower (bcc) density limits for unstrained crystal structures, where those limit densities are duals [Eq. (5.8)]. In particular, conclusion (1) indicates that the Debye approximation for the phonon spectra is qualitatively inapplicable to the Gaussian core model at high density.

As mentioned in the Introduction, previous work[6,10] has established that the Gaussian core model in two and in three dimensions exhibits negative thermal expansion at intermediate and high density, encompassing both crystal and fluid phases. This observation contrasts with familiar examples such as water and silica, where the negative thermal expansion can logically be attributed to the presence of nonspherical dynamical units that experience strongly directional forces. Interparticle forces are spherically symmetric in the present case and the phonon frequencies that they create in the crystal possess density dependences that produce negative thermal expansion, at least at low temperature. Property (1) listed above implies that many of the mode Grüneisen constants[19]

$$\frac{\partial \ln \omega_j(\mathbf{k})}{\partial \ln \rho} = \gamma_j(\mathbf{k}) \qquad (6.1)$$

can be strongly negative and through their contribution to the pressure equation of state[19] can thereby produce the observed effect. The corresponding phenomenon in the higher-temperature fluid may be roughly analogous, but must require a more complicated explanation, because considerable intrabasin anharmonicity is present.

The loss of mechanical stability as strained lattices are densified, discussed in Sec. IV above and documented in Table I for the triangular lattice, is a special case of the property (c) mentioned in the Introduction. That convolution smoothing property as density increases has the effect of eventually eliminating all but the most stable inherent structures and their surrounding basins. In two dimensions, only the $N!$ permutation-equivalent basins for the unstrained tri-

angular lattice would presumably survive unbounded compression, while in three dimensions it would be the $N!$ inherent structures and basins for the undistorted body-centered-cubic lattice. If this hypothesis is correct, it raises an engaging basic question about the fate of the first-order melting transition in the high-compression asymptotic regime (within which the melting temperature is declining toward zero). Survival of a melting phase transition, with only one type of multidimensional basin present, would then necessarily be an intrabasin anharmonic phenomenon. Indeed, the theoretical possibility of intrabasin melting has been previously explored (though not in connection with the Gaussian core model).[20] Whether this elementary view of melting in the high-compression limit is valid or whether a more delicate balancing of basin elimination and interbasin thermal excitation is involved will have to await subsequent mathematical analysis.

APPENDIX A

One of the standard Jacobi θ functions is defined as follows:[14]

$$\vartheta_3(z,q) = 1 + 2\sum_{n=1}^{\infty} q^{n^2} \cos(2nz). \qquad (A1)$$

If one sets

$$q = \exp(-a^2), \quad 2z = ka, \qquad (A2)$$

then Eq. (A1) leads to the expression

$$\vartheta_3[ka/2, \exp(-a^2)] - 1 = 2\sum_{n=1}^{\infty} \exp(-n^2 a^2)\cos(kan). \qquad (A3)$$

In addition, Eq. (A1) also allows one to conclude [subject to substitutions (A2)]

$$-(\partial/\partial \ln \ln q)\vartheta_3(z,q) = 2\sum_{n=1}^{\infty} n^2 a^2 \exp(-n^2 a^2)\cos(kan). \qquad (A4)$$

Relations (A3) and (A4) then allow the determining Eq. (2.3) for phonon frequencies in the one-dimensional GCM to be formally expressed in terms of the ϑ_3 function:

$$\omega^2(k) = 2\{[2(\partial/\partial \ln \ln q) - 1]$$
$$\times [\vartheta_3(0,q) - \vartheta_3(ka/2,q)]\}_{q=\exp(-a^2)}. \qquad (A5)$$

In this formula $a = 1/\rho$ represents the nearest-neighbor separation in the linear chain.

Page 476 of Ref. 14 presents the following identity:

$$\sum_{n=-\infty}^{\infty} \exp(n^2 \pi i \tau + 2niz) = (-i\tau)^{-1/2} \sum_{n=-\infty}^{\infty} \exp\left[\frac{(z-n\pi)^2}{\pi i \tau}\right]. \qquad (A6)$$

For the one-dimensional GCM phonon study it is convenient to set

$$\pi i \tau = -a^2, \quad 2z = ka. \tag{A7}$$

Upon making these substitutions and rearranging the result, Eq. (A1) leads to the following:

$$1 + 2\sum_{n=1}^{\infty} \exp(-n^2 a^2)\cos(nka)$$

$$= (\pi^{1/2}/a)\exp(-k^2/4)\left[1 + 2\sum_{n=1}^{\infty} \exp(-n^2\pi^2/a^2) \right.$$

$$\left. \times \cosh(n\pi k/a) \right]. \tag{A8}$$

Apply the differential operator $-\partial^2/\partial k^2$ to both sides of this last expression to obtain

$$2\sum_{n=1}^{\infty} n^2 a^2 \exp(-n^2 a^2)\cos(nka)$$

$$= \left(\frac{\pi^{1/2}}{a}\right)\exp\left(-\frac{k^2}{4}\right)\left\{ \frac{1}{2} - \frac{k^2}{4} \right.$$

$$+ \sum_{n=1}^{\infty} \exp\left(-\frac{k^2}{4}\right)\left[\frac{2\pi nk}{a}\sinh\left(\frac{n\pi k}{a}\right) \right.$$

$$\left. \left. + \left(1 - \frac{k^2}{2} - \frac{2\pi^2 n^2}{a^2} \right)\cosh\left(\frac{n\pi k}{a}\right) \right] \right\}. \tag{A9}$$

Equations (A8) and (A9) suffice to convert Eq. (2.3) of the main text to the alternative form Eq. (2.4), after replacing a with $1/\rho$.

---

[1] P. J. Flory and W. R. Krigbaum, J. Chem. Phys. **18**, 1086 (1950).

[2] C. N. Likos, M. Schmidt, H. Löwen, M. Ballauff, D. Pötschke, and P. Lindner, Macromolecules **34**, 2914 (2001).

[3] A. Lang, C. N. Likos, M. Watzlawek, and H. Löwen, J. Phys.: Condens. Matter **12**, 5087 (2000).

[4] C. N. Likos, Phys. Rep. **348**, 267 (2001), Sec. 3.5.

[5] F. H. Stillinger, J. Chem. Phys. **70**, 4067 (1979).

[6] F. H. Stillinger and T. A. Weber, J. Chem. Phys. **74**, 4015 (1981).

[7] T. A. Weber and F. H. Stillinger, J. Chem. Phys. **74**, 4020 (1981).

[8] F. H. Stillinger, Phys. Rev. B **20**, 299 (1979).

[9] F. H. Stillinger, J. Chem. Phys. **65**, 3968 (1976).

[10] F. H. Stillinger and D. K. Stillinger, Physica A **244**, 358 (1997).

[11] A. A. Louis, P. G. Bolhuis, and J. P. Hansen, Phys. Rev. E **62**, 7961 (2000).

[12] F. Seitz, *The Modern Theory of Solids* (McGraw-Hill, New York, 1940), pp. 104–117.

[13] L. Brillouin, *Wave Propagation in Periodic Structures* (Dover, New York, 1953).

[14] E. T. Whittaker and G. N. Watson, *A Course of Modern Analysis* (Cambridge University Press, Cambridge, England, 1952), Chap. XXI.

[15] N. W. Ashcroft and N. D. Mermin, *Solid State Physics* (Holt, Reinhart, and Winston, New York, 1976), pp. 86–94.

[16] H. P. Myers, *Introductory Solid State Physics*, 2nd ed. (Taylor & Francis, London, 1997), p. 127.

[17] L. D. Landau and E. M. Lifshitz, *Theory of Elasticity* (Pergamon Press, London, 1959), Sec. 10.

[18] F. H. Stillinger, Phys. Rev. E **66**, 066125 (2002).

[19] R. Kubo, *Statistical Mechanics* (North-Holland, Amsterdam, 1965), p. 137.

[20] F. H. Stillinger, Physica A **177**, 79 (1991).